

# Three-dimensional lattice structure formed in a binary system with DNA nanoparticles

メタデータ	言語: eng 出版者: 公開日: 2017-12-05 キーワード (Ja): キーワード (En): 作成者: メールアドレス: 所属:
URL	<a href="http://hdl.handle.net/2297/48424">http://hdl.handle.net/2297/48424</a>

# Three-Dimensional Lattice Structure Formed in a Binary System with DNA Nanoparticles

Keno Kawasaki<sup>1</sup>, Hiroyasu Katsuno<sup>2</sup>, and Masahide Sato<sup>3</sup>

<sup>1</sup>*Graduate School of Natural Science and Technology, Kanazawa University,  
Kakuma-machi, Kanazawa 920-1192, Japan*

<sup>2</sup>*Department of Physical Sciences, Ritsumeikan University, 1-1-1 Noji Higashi,  
Kusatsu, Shiga 525-8577, Japan*

<sup>3</sup>*Information Media Center, Kanazawa University, Kakuma-machi, Kanazawa  
920-1192, Japan*

Keeping the formation of lattice structures by nanoparticles covered with DNA in mind, we carry out Brownian dynamics simulations and study three-dimensional lattice structures formed by two species of particles. In our previous study [H. Katsuno, Y. Maegawa, and M. Sato, J. Phys. Soc. Jpn. **85**, 074605 (2016)], we used the Lennard–Jones potential and studied two-dimensional structures formed in a binary system. When the interaction length between the different species,  $\sigma'$ , is shorter than that between the same species,  $\sigma$ , the lattice structure changes with the ratio  $\sigma'/\sigma$ . In this paper, we use the same potential and study the formation of three-dimensional structures. With decreasing ratio  $\sigma'/\sigma$ , the mixture of the face-centered-cubic (fcc) structure and hexagonal-close-packed (hcp) structure is changed to the body-centered-cubic (bcc) structure and the NaCl structure.

## 1. Introduction

Using nanoparticles covered with DNA strands, which we call DNA nanoparticles, as building blocks is a promising method for creating various nanostructures because the particle size, the particle shape, and the interaction between particles are controlled easily. In experiments,<sup>1–7)</sup> linker strands are used to connect the DNA nanoparticles. When a self-complementary linker is used, the system becomes a single-component system and the face-centered-cubic (fcc) structure is formed. With two different non-self-complementary linkers, the system becomes a binary system. The particles with different types of linkers attract each other, and the body-centered-cubic (bcc) structure

is formed. The NaCl structure is also formed when both the self-complementary linkers and the non-self-complementary linkers are added to DNA nanoparticles.<sup>4)</sup> It is possible to form more complicated structures such as CsCl, AlB<sub>2</sub>, Cr<sub>3</sub>Si, and Cs<sub>6</sub>C<sub>60</sub> lattices when DNA nanoparticles with two different sizes are used as building blocks.<sup>5)</sup>

Many lattice structures have been formed in experiments,<sup>1-7)</sup> and some rules for designing the lattice structures have been proposed.<sup>4)</sup> However, there has been little progress in obtaining a theoretical understanding of the mechanism for forming the lattice structures, which is probably due to difficulties in modeling the interaction between the DNA nanoparticles.<sup>8,9)</sup> As a first step, it is necessary to study the formation of lattice structures, assuming a concrete interaction between the particles. Thus, in our previous paper,<sup>10)</sup> we introduced a simple system and studied two-dimensional structures formed in a binary system, in which the Lennard–Jones (LJ) potential was used as the interaction potential between particles. In the model, we neglected the difference in the interaction strength and focused on the difference in the interaction length: we assumed that the interaction length between the different species,  $\sigma'$ , is smaller than that between the same species,  $\sigma$ . We carried out Brownian dynamics simulations with various ratios  $\sigma'/\sigma$  and showed that various two-dimensional structures were formed.

Experimentally, the three-dimensional lattice structures formed by DNA nanoparticles<sup>1-5)</sup> have been studied more than the two-dimensional structures.<sup>6,7)</sup> Thus, in this paper, we use the same model as that used in our previous study<sup>10)</sup> and investigate the formation of three-dimensional structures. We carry out Brownian dynamics simulations to show how the three-dimensional structure changes with the ratio  $\sigma'/\sigma$ . In Sect. 2, we introduce our model. In Sect. 3, we estimate the interaction energies for some structures and consider the dependence of the lattice structures on the ratio  $\sigma'/\sigma$ . Then, we carry out simulations with different values of  $\sigma'/\sigma$ . We calculate the radial distribution function and local orientation symmetries to determine the structure formed in the binary system. In Sect. 4, we summarize our results and give a brief discussion.

## 2. Model

We consider nanoparticles moving in a solution. The particles are subjected to viscous resistance and random thermal noise from the solution. The equation of motion for the  $i$ th particle is given by

$$m \frac{d^2 \mathbf{r}_i}{dt^2} = -\xi \frac{d\mathbf{r}_i}{dt} + \mathbf{F}_i + \mathbf{F}_i^B, \quad (1)$$

where  $m$  is the particle mass,  $\mathbf{r}_i$  is the position of the  $i$ th particle, and  $\xi$  is the frictional coefficient.  $\mathbf{F}_i^{\text{B}}$  represents the thermal noise satisfying  $\langle \mathbf{F}_i^{\text{B}} \rangle = \mathbf{0}$  and  $\langle F_{i,k}^{\text{B}}(t) F_{j,l}^{\text{B}}(t') \rangle = 2\xi k_{\text{B}} T \delta_{ij} \delta_{kl} \delta(t-t')$ , where  $F_{i,k}^{\text{B}}(t)$  represents the component of the thermal noise acting on the  $i$ th particle in the  $k$ -direction.  $\mathbf{F}_i$  is the sum of the inertial forces for the  $i$ th particle, which is expressed by the interaction potential  $U(r_{ij})$  as

$$\mathbf{F}_i = \sum_{i \neq j} \nabla U(r_{ij}), \quad (2)$$

where  $r_{ij} = |\mathbf{r}_i - \mathbf{r}_j|$ . We use the LJ potential as the interaction potential:

$$U(r_{ij}) = 4\epsilon_{ij} \left\{ \left( \frac{\sigma_{ij}}{r_{ij}} \right)^{12} - \left( \frac{\sigma_{ij}}{r_{ij}} \right)^6 \right\}, \quad (3)$$

where  $\epsilon_{ij}$  and  $\sigma_{ij}$  represent the interaction strength and interaction length, respectively. The interaction is repulsive when  $r_{ij} < 2^{1/6} \sigma_{ij}$ . With decreasing  $r_{ij}$ , the repulsive force increases sharply. Particles are subjected to an attractive force when  $r_{ij} > 2^{1/6} \sigma_{ij}$ . The attraction decreases gradually with increasing the distance between two particles and becomes negligible when  $r_{ij} \leq 3\sigma_{ij}$ . Thus, owing to its simplicity, the LJ potential is reasonably satisfactory as the interaction potential for hard nanoparticles covered with fine and flexible DNA strands.

In our simulations, we consider a system consisting of two species, where the numbers of the two species are the same. In general, both  $\epsilon_{ij}$  and  $\sigma_{ij}$  may depend on the combination of the  $i$ th and  $j$ th particles, but we neglect the difference in  $\epsilon_{ij}$  for simplicity. We assume that the interaction length for a pair of the same species,  $\sigma$ , is larger than that for a pair of the different species,  $\sigma'$ , and study how the lattice structure changes with the ratio  $\sigma'/\sigma$ .

We assume that the viscosity is very large so that we can solve Eq. (1) numerically neglecting  $md^2\mathbf{r}/dt^2$ . A simple difference equation for Eq. (1) is given by<sup>11)</sup>

$$\tilde{\mathbf{r}}_i(\tilde{t}_{n+1}) = \tilde{\mathbf{r}}_i(\tilde{t}_n) + \tilde{\mathbf{F}}_i \Delta \tilde{t} + \Delta \tilde{\mathbf{r}}_i^{\text{B}}, \quad (4)$$

where  $\tilde{\mathbf{r}}_i = \mathbf{r}_i/\sigma$ ,  $\tilde{t}_n = \epsilon t_n / (\xi \sigma^2)$ ,  $\tilde{\mathbf{F}}_i = \sigma \mathbf{F}_i / \epsilon$ , and  $\tilde{t}_{n+1} = \tilde{t}_n + \Delta \tilde{t}$ . The displacement by the random force,  $\Delta \tilde{\mathbf{r}}_i^{\text{B}}$ , satisfies  $\langle \Delta \tilde{\mathbf{r}}_i^{\text{B}} \rangle = \mathbf{0}$  and  $\langle \Delta \tilde{r}_{i,k}^{\text{B}}(t_n) \Delta \tilde{r}_{j,l}^{\text{B}}(t_m) \rangle = 2k_{\text{B}} T \delta_{ij} \delta_{kl} \delta_{mn} / \epsilon$ , where  $\Delta \tilde{r}_{i,k}^{\text{B}}(t_n)$  represents the component of  $\Delta \tilde{\mathbf{r}}_i^{\text{B}}$  in the  $k$ th direction.

To specify lattice structures formed by the simulations, we estimate the radial distribution function  $g(r)$  defined as

$$g(r) = \frac{1}{N} \sum_m^{N_s} \sum_i^N \frac{n_{i,m}}{4\pi r^2 \delta r}, \quad (5)$$

where  $n_{i,m}$  represents the number of particles between distances  $r$  and  $r + \delta r$  for the  $i$ th particle in the  $m$ th run.  $N$  and  $N_s$  represent the particle number in a sample and the sample number, respectively. In our estimation,  $\delta r$  is set to  $10^{-2}$ .

**Table I.**  $Q_4$  and  $Q_6$  in perfectly symmetric configurations for the face-centered-cubic (fcc) structure, the hexagonal-close-packed (hcp) structure, the body-centered-cubic (bcc) structure, and the simple cubic (sc) structure.<sup>14)</sup>

	fcc	hcp	bcc	sc
$Q_4$	0.190	0.097	0.509	0.764
$Q_6$	0.575	0.484	0.629	0.354

We also estimate order parameters  $Q_4(i)$  and  $Q_6(i)$ ,<sup>12,13)</sup> which represent the local orientational symmetry around the  $i$ th particle.  $Q_l(i)$  is defined as

$$Q_l(i) = \sqrt{\frac{4\pi}{2l+1} \sum_{m=-l}^l |q_{l,m}(i)|^2}, \quad (6)$$

where  $q_{l,m}(i)$  is given by

$$q_{l,m}(i) = \frac{1}{n_n} \sum_{j=1}^{n_n} Y_l^m(\theta_{ij}, \phi_{ij}). \quad (7)$$

In Eq. (7),  $n_n$  represents the number of neighbors of the  $i$ th particle,  $Y_l^m(\theta_{ij}, \phi_{ij})$  is the spherical harmonics, and  $\theta_{ij}$  and  $\phi_{ij}$  represent the polar and azimuthal angles for  $\mathbf{r}_j - \mathbf{r}_i$ , respectively. The values of  $Q_4$  and  $Q_6$  in perfectly symmetric configurations for some lattice structures are shown in Table I.<sup>14)</sup>

### 3. Results

Before carrying out simulations, we set the distance between the same species to  $2^{1/6}\sigma$  and consider the relationship between  $\sigma'/\sigma$  and the interaction energy for the structures in Table I. The close-packed-structures, i.e., the fcc structure and the hcp structure, are formed when the connection between the different species is equivalent to that between the same species. If we neglect the effects of the third- and higher-order neighbors, the interaction energy for the hcp structure is the same as that for the fcc structure. The distances for the nearest neighbors and the next nearest neighbors are  $2^{1/6}\sigma$  and  $\sqrt{2} \times 2^{1/6}\sigma$ , respectively. Hereafter, we express  $2^{1/6}\sigma$  as  $r_0$ . If we assume that

the two types of species are randomly located at the lattice positions,  $E_{LJ}^{\text{fcc,hcp}}$  satisfies

$$\begin{aligned} \frac{E_{LJ}^{\text{fcc,hcp}}}{2\epsilon} &= \left[ \frac{N_{\text{nn}}}{2} \left\{ \left( \frac{1}{2^{1/6}} \right)^{12} - \left( \frac{1}{2^{1/6}} \right)^6 \right\} + \frac{N_{\text{nnn}}}{2} \left\{ \left( \frac{1}{2^{1/6}\sqrt{2}} \right)^{12} - \left( \frac{1}{2^{1/6}\sqrt{2}} \right)^6 \right\} \right] \\ &+ \left[ \frac{N_{\text{nn}}}{2} \left\{ \left( \frac{s}{2^{1/6}} \right)^{12} - \left( \frac{s}{2^{1/6}} \right)^6 \right\} + \frac{N_{\text{nnn}}}{2} \left\{ \left( \frac{s}{2^{1/6}\sqrt{2}} \right)^{12} - \left( \frac{s}{2^{1/6}\sqrt{2}} \right)^6 \right\} \right], \quad (8) \end{aligned}$$

where  $s = \sigma'/\sigma$ , and the numbers of nearest neighbors,  $N_{\text{nn}}$ , and next nearest neighbors,  $N_{\text{nnn}}$  are 12 and 6, respectively.

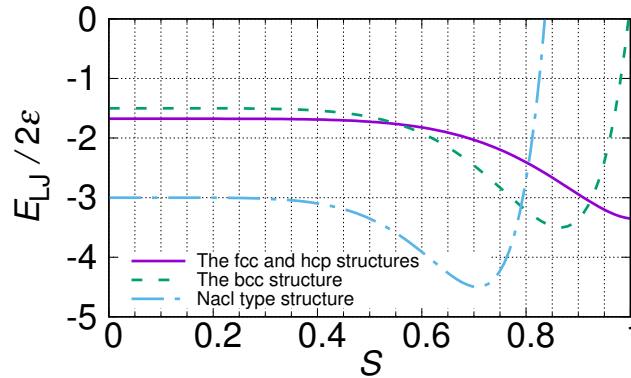
To form the bcc structure, the most suitable distance between the different species is given by  $\sqrt{3}r_0/2$ . When we take the interaction between particles into account up to the next nearest neighbors, the interaction energy per particle,  $E_{LJ}^{\text{bcc}}$ , satisfies

$$\frac{E_{LJ}^{\text{bcc}}}{2\epsilon} = \left[ N_{\text{nn}} \left\{ \left( \frac{2s}{2^{1/6}\sqrt{3}} \right)^{12} - \left( \frac{2s}{2^{1/6}\sqrt{3}} \right)^6 \right\} + N_{\text{nnn}} \left\{ \left( \frac{1}{2^{1/6}} \right)^{12} - \left( \frac{1}{2^{1/6}} \right)^6 \right\} \right], \quad (9)$$

where  $N_{\text{nn}} = 8$  and  $N_{\text{nnn}} = 6$ . The NaCl lattice is the most suitable structure when the distance between the different species is  $\sqrt{2}r_0/2$ . In the case, the interaction energy  $E_{LJ}^{\text{sc}}$  is given by

$$\frac{E_{LJ}^{\text{sc}}}{2\epsilon} = \left[ N_{\text{nn}} \left\{ \left( \frac{2s}{2^{1/6}\sqrt{2}} \right)^{12} - \left( \frac{2s}{2^{1/6}\sqrt{2}} \right)^6 \right\} + N_{\text{nnn}} \left\{ \left( \frac{1}{2^{1/6}} \right)^{12} - \left( \frac{1}{2^{1/6}} \right)^6 \right\} \right], \quad (10)$$

where  $N_{\text{nn}} = 6$  and  $N_{\text{nnn}} = 12$ .



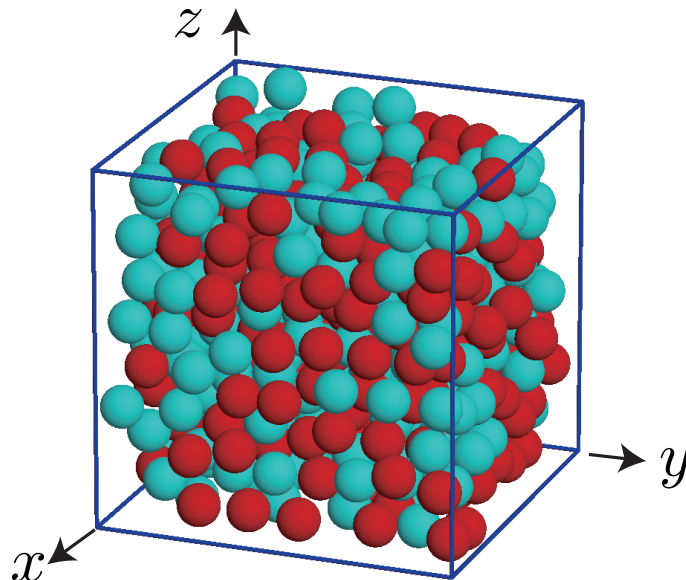
**Fig. 1.** (color online) Dependence of  $E_{LJ}$  on the ratio  $s$  for the close-packed structures, the bcc structure, and the NaCl structure.

Figure 1 shows the dependency of  $E_{LJ}^{\text{bcc}}$ ,  $E_{LJ}^{\text{fcc,hcp}}$ , and  $E_{LJ}^{\text{sc}}$  on  $s$ . The structure giving the minimum energy changes from the close-packed structures to the bcc structure then the NaCl structure with decreasing  $s$ ; the close-packed structures, the bcc structure, and the NaCl structure are formed when  $0.92 \leq s$ ,  $0.79 \leq s \leq 0.92$ , and  $s \leq 0.79$ ,

respectively.

In the following, we carry out Brownian dynamics simulations with different values of  $s$  and investigate the structures. In our simulations,  $k_B T/\epsilon$  is set to 0.1. We use a small system owing to limited numerical resources. The number of particles is  $N = 500$  and the number of each type of particle is  $N/2 = 250$ . A scaled cubic box with a side length of 8 is used as the simulation box with the periodic boundary condition. If we regard  $\sigma$  as the radius of the particles, the volume fraction is estimated to be 0.5. Initially,  $N$  particles are placed at random in the system. After moving the particles for a long time, we investigate the lattice structure.

### 3.1 Results for $s = 0.95$



**Fig. 2.** (color online) Snapshot of structure formed with  $s = 0.95$ , where the two species are distinguished by the difference in color.

From Fig. 1, the fcc structure, the hcp structure, or their mixture is expected to be formed when  $0.92 \leq s$ . To confirm our expectation, we carried out 40 individual runs with  $s = 0.95$  until  $t \simeq 4.8 \times 10^4$  and obtained 15 ordered samples. Sharp peaks in the radial distribution function  $g(r)$  appeared at  $t \sim 10^3$  in the ordered samples, but the sharp peaks did not appear in the other samples when  $t > 10^4$ . Thus, we did not carry out longer simulations and averaged  $g(r)$  over the ordered samples. In Fig. 2, we show a typical snapshot in the ordered case, where we distinguish the two species

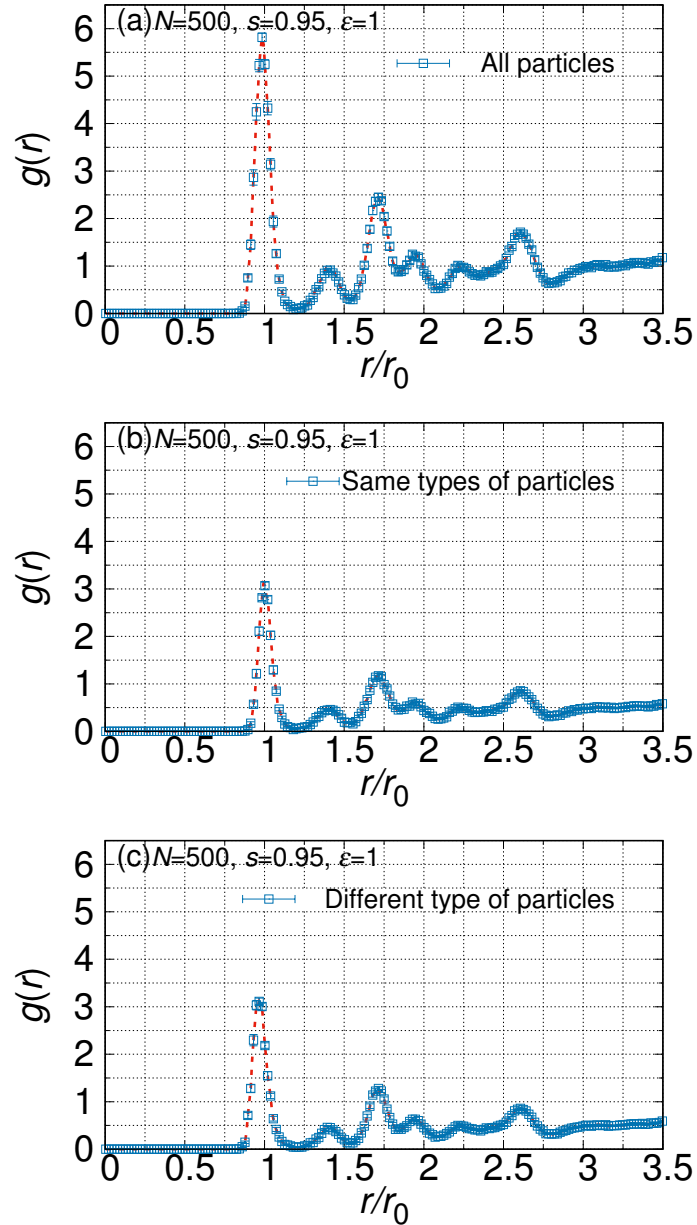


**Fig. 3.** (color online) (a) Radial distribution function  $g(r)$ , (b) contributions of the same species to  $g(r)$ , and (c) that of different species to  $g(r)$  for  $s = 0.95$ . Results are averaged over 15 ordered samples. Error bars represent standard errors.

by the difference in color. Figure 3 shows  $g(r)$  averaged over 15 ordered samples. The contributions of the same and different species to  $g(r)$  are shown in Figs. 3(b) and 3(c), respectively. Since the positions and heights of the peaks are the same in these figures, the two species are mixed randomly, which seems to agree with Fig. 2. In Fig. 3(a), the first peak clearly appears at  $r = r_0$ . When we count  $N_{nn}$  within  $1.16r_0$ , the positions of the second and third peaks are  $1.47r_0$  and  $1.73r_0$ , respectively. Since the positions of

these peaks are given by  $\sqrt{2}r_0$  and  $\sqrt{3}r_0$  for the fcc structure and  $\sqrt{2}r_0$  and  $2\sqrt{2}r_0/\sqrt{3}$  for the hcp structure, the fcc structure appears to be formed in the samples. However, owing to the broadness of the peaks, we cannot state clearly that the hcp structure is not formed. Thus, we estimate  $Q_4$  and  $Q_6$ .

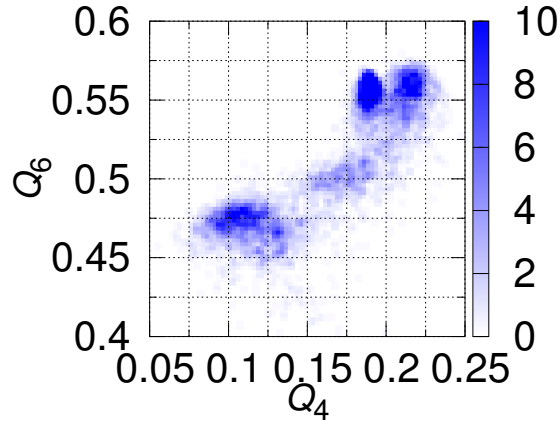


**Fig. 4.** (color online) Distribution of  $Q_4$  and  $Q_6$  for  $s = 0.95$ , in which the particles with nine or fewer neighbors are neglected. The distribution shows the sum of 15 ordered samples.

Figure 4 shows the distribution of  $Q_4$  and  $Q_6$ . When  $N_n$  is small, we cannot calculate the order parameters correctly. Thus, we estimated  $Q_4$  and  $Q_6$  for the particles with  $N_n \geq 10$  in Fig. 4. High-density regions appear in the top-right and bottom-left, which shows that both the fcc and hcp structures are formed by the mixture. The top-right region is larger than that in the bottom-left one; thus, the fcc structure is more dominant than the hcp structure, which is consistent with  $g(r)$ .

### 3.2 Results for $s = 0.85$

When  $0.79 \leq s \leq 0.92$ , the structure expected from Fig. 1 is the bcc lattice. Here, to confirm the formation of the bcc structure, we carry out a simulation with  $s = 0.85$  at  $t \simeq 3.1 \times 10^3$ . Figure 5 shows a typical snapshot. We find that the two species are mixed well, but we cannot confirm the formation of the bcc structure from the figure. Thus, we calculate  $g(r)$  to investigate the formation of the bcc structure. Figure 6 shows  $g(r)$  with  $s = 0.85$ . The first peak at  $0.78r_0$  is formed by the different species [Fig. 6(c)]. The second peak, which is formed by the same species, appears at  $r = 0.98r_0$  [Fig. 6(b)]. The third peak at  $1.63r_0$  is formed by both the same and different species [Figs. 6(b) and 6(c)]. The structure appears to be the bcc structure, but the positions of these

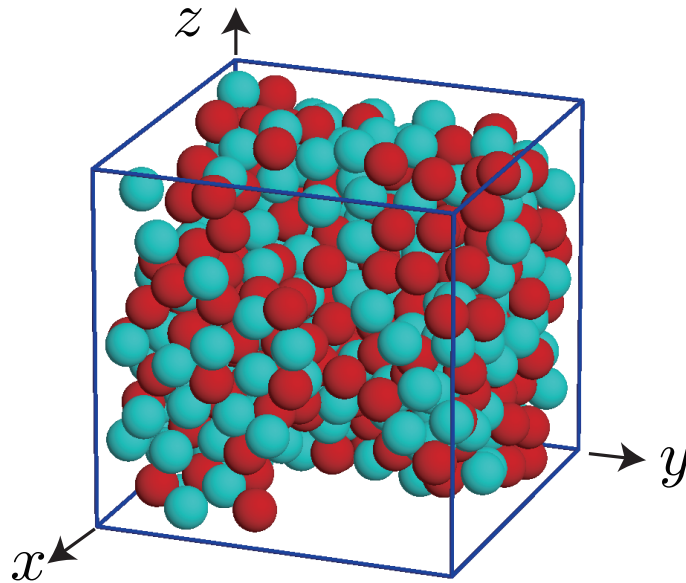


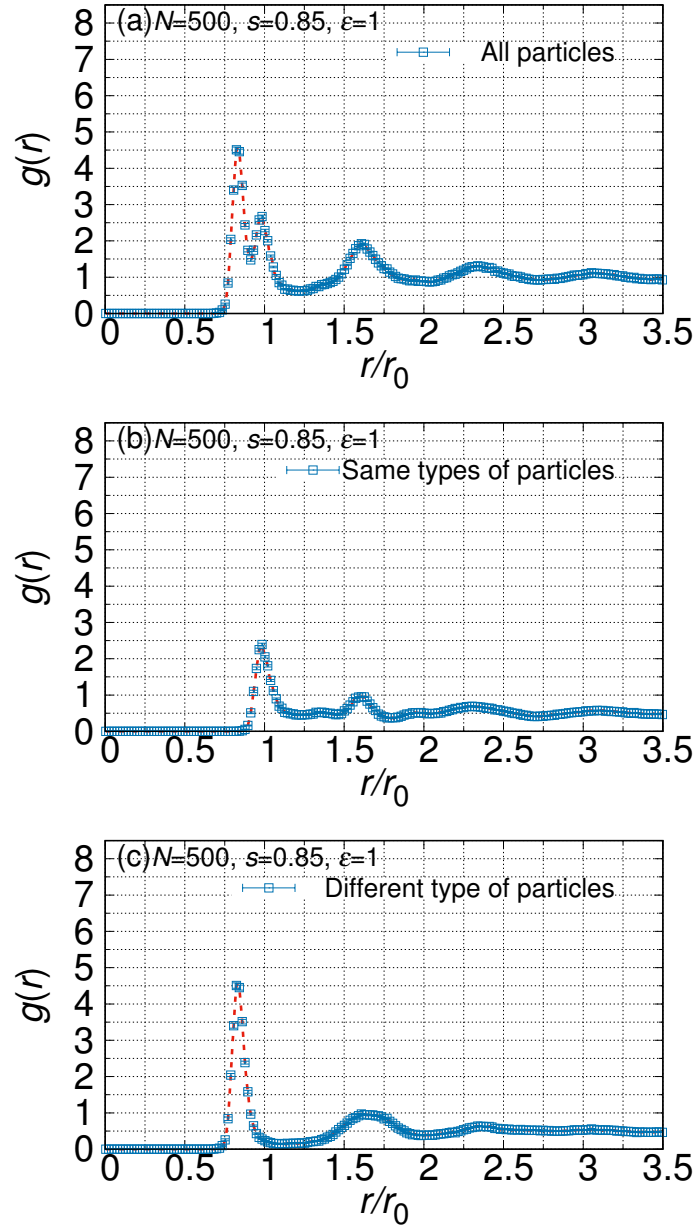
**Fig. 5.** (color online) Snapshot of the structure with  $s = 0.85$ , where the two species are distinguished by the difference in color.

peaks are slightly misaligned from those for the perfect bcc structure. We cannot find the fourth and subsequent peaks in Fig. 6(a): thus, long-range ordering does not occur.

The misalignment from the bcc structure is also confirmed from  $Q_4$  and  $Q_6$ . The ratios of the numbers of particles with eight, seven, and six neighbors to  $N$  are 0.5%, 11%, and 39%, respectively. Since the number of particles having eight or seven neighbors is small, we estimate  $Q_4$  and  $Q_6$  for the particles with  $N_n \geq 6$ . Figure 7 shows the distribution of  $Q_4$  and  $Q_6$ . If the perfect bcc structure is formed,  $Q_4$  and  $Q_6$  are 0.509 and 0.629, respectively. In Fig. 7, however,  $Q_4$  is distributed broadly and  $Q_6$  is shifted to the lower side. In addition to  $g(r)$ , the local orientational symmetry also deviates from that in the bcc structure.

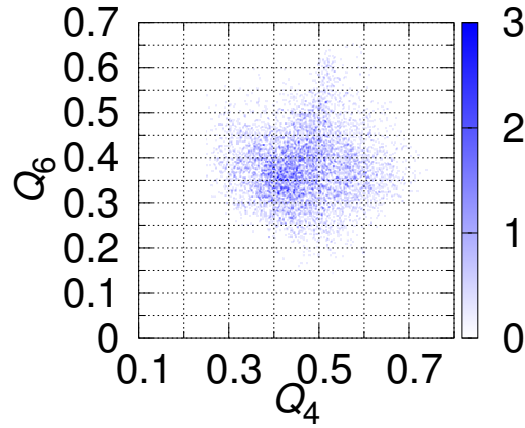
### 3.3 Results for $s = 0.7$

Figure 8 shows a snapshot for  $s = 0.7$  at  $t \simeq 1.1 \times 10^3$ , where we expect the formation of the NaCl type lattice. In the figure, the two species appear to form a regular structure. To confirm whether the regular structure is the NaCl structure, we calculate the radial distribution function. Figure 9(a) shows  $g(r)$  for  $s = 0.7$ . Peaks appear at  $r = 0.7r_0$ ,  $r_0$ ,  $1.2r_0$ ,  $1.4r_0$ ,  $1.6r_0$ , and  $1.7r_0$ . The first, third, and fifth peaks consist of the different species [Fig. 9(c)] and the second, fourth, and sixth peaks consist of the same species [Fig. 9(b)]. From these peaks, we confirm that the NaCl structure



**Fig. 6.** (color online) (a) Radial distribution function  $g(r)$ , (b) contribution of the same species to  $g(r)$ , and (c) that of different species to  $g(r)$  for that  $s = 0.85$ . Results are averaged over 40 runs. Error bars represent standard errors.

with the lattice constant  $1.4r_0$  is formed in the system. We calculate  $Q_4$  and  $Q_6$  for the particles with  $N_{nn} \geq 5$ . Figure 10 shows the distribution of  $Q_4$  and  $Q_6$ . Although there are two spots, they are mainly distributed around  $Q_4 = 0.75$  and  $Q_6 = 0.35$ . From Table I, we can confirm that the local orientational order parameters also show the formation of the simple cubic lattice, which agrees with the formation of the NaCl lattice.



**Fig. 7.** (color online) Distribution of  $Q_4$  and  $Q_6$  for  $s = 0.85$ , which is the sum of 40 samples.

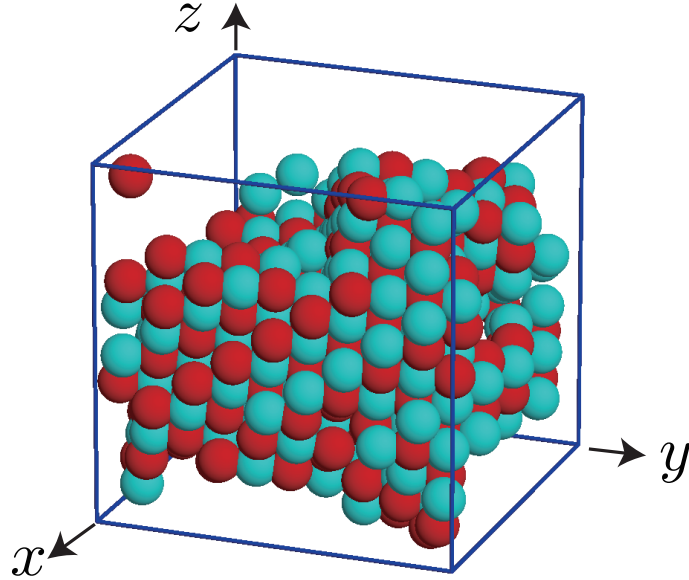


**Fig. 8.** (color online) Snapshot of the structure with  $s = 0.7$ , where the two species are distinguished by the difference in color.

### 3.4 Results for $s = 0.6$

Small values of  $s$  do not seem to be realistic because of the steric hindrance. However, some structures are formed for the small values of  $s$  in the two-dimensional system.<sup>10)</sup> Thus, we investigate the case that  $s = 0.6$ . Figure 11 shows the radial distribution function for  $s = 0.6$  at  $t \simeq 2.2 \times 10^3$ . The first peak formed by the different species appears at  $r = 0.6r_0$  and the second peak formed by the same species appears at  $r = r_0$ , but the other peaks do not appear clearly.  $g(r)$  has a liquidlike form; thus, the lattice

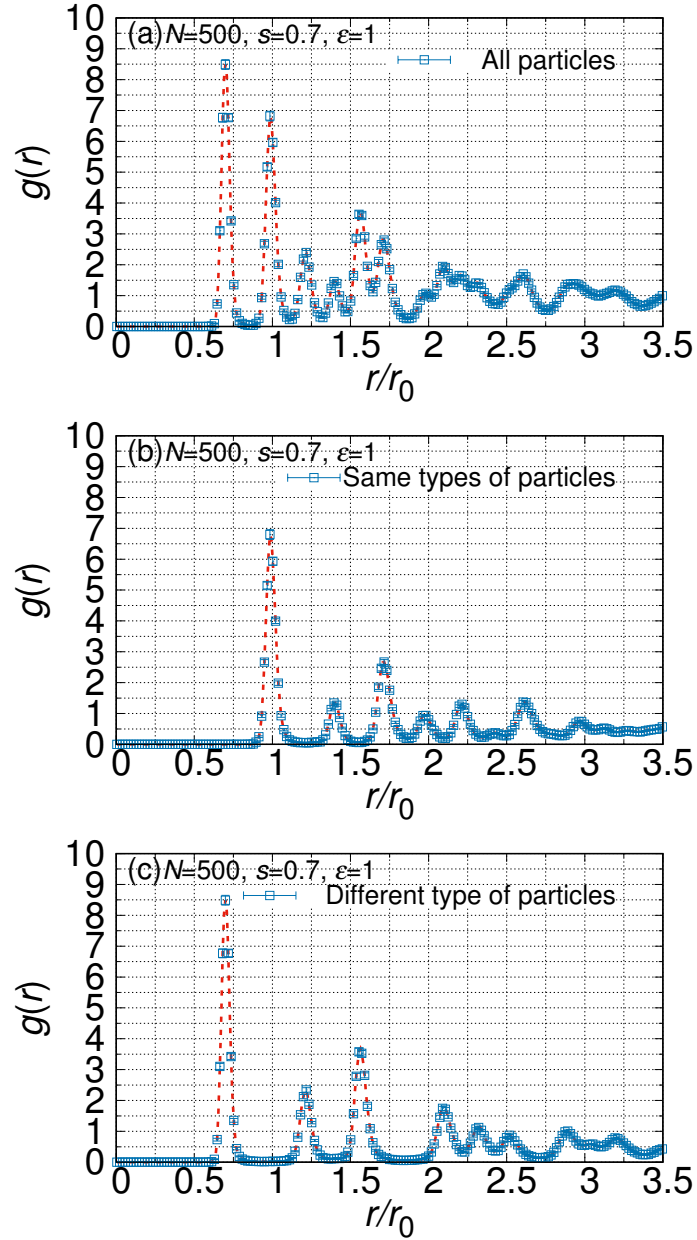


**Fig. 9.** (color online) (a) Radial distribution function  $g(r)$ , (b) contributions of the same species to  $g(r)$ , and (c) that of different species to  $g(r)$  for  $s = 0.7$ . (a) shows  $g(r)$ , and (b) and (c) show the contributions of the same species and different species to  $g(r)$ , respectively. Results are averaged over 40 runs. Error bars represent standard errors.

structure is not formed. We also carried out simulations for  $s = 0.5$  and  $s = 0.4$ . In both cases, the radial distribution function showed the formation of a similar liquidlike structure. Thus, in our simulations, the formation of a lattice structure was not observed with small values of  $s$ .

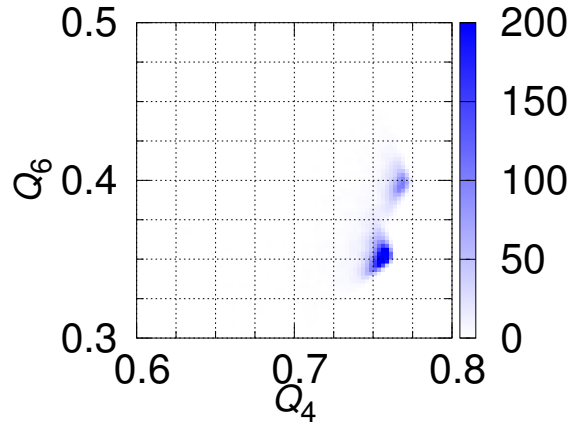


**Fig. 10.** (color online) Distribution of  $Q_4$  and  $Q_6$  for  $s = 0.7$ , which is the sum of the 40 samples.

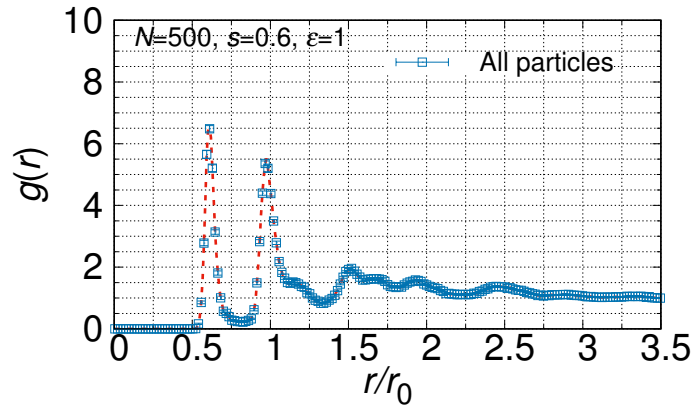


**Fig. 11.** (color online) Radial distribution function for  $s = 0.6$ . The data are averaged over 40 runs. Error bars represent standard errors.

#### 4. Summary and Discussion

In this paper, keeping DNA nanoparticles in mind, we carried out Brownian dynamics simulations and studied the three-dimensional structure in a binary system. We set the interaction length between the different species,  $\sigma'$ , to be smaller than that between the same species,  $\sigma$ . The formed structure changes with  $s$ , which is defined as  $s = \sigma'/\sigma$ : a mixture of the fcc and hcp structures, the bcc structure, and the NaCl-type structure were formed for  $s = 0.95$ ,  $0.85$ , and  $0.7$ , respectively. These structures agreed with the lattice expected from a simple energy estimation.

When  $s = 0.95$ , the simulation time was more than 10 times that in the cases with  $s = 0.85$ ,  $0.75$ , and  $0.6$ , but the ordered state was formed in only 15 samples.

Long calculation time is probably needed for the disordered samples to relax to the ordered state. Owing to our limited computational resources, we did not carry out long calculation and estimated the radial distribution function  $g(r)$  for the ordered samples. A mixture of the hcp and fcc structures was formed in the ordered samples although the fcc structure is more stable than the hcp structure.<sup>15)</sup> When we carried out simulations with  $s = 1.0$ , a mixture of the hcp and fcc structures was formed. Thus, the formation of a metastable structure is not caused by the deviation of  $s$  from the most suitable value. Although we carried out the simulations with a small system, a longer time is probably necessary to form the most stable structure.

When  $s = 0.85$ , the formation of the bcc structure was expected from the rough estimation of the interaction energy as shown in Fig. 1. Judging from the peaks in the radial distribution function, the bcc structure appears to be formed locally, but a long-range order is not formed. In previous experiments,<sup>1-5)</sup> the attraction between the same species was neglected when the bcc structure was formed. On the other hand, the attractive force acts on the same species in our simulation. The attraction between the same species may prevent the formation of the long-range order. In future, we intend to confirm the effect of attraction between the same species on the lattice structure.

Since both the attraction between the same species and that between the different species are taken into account, our model is close to a system in which both self-complementary linkers and non-self-complimentary linkers are added to DNA nanoparticles.<sup>4)</sup> The interaction in our model will probably be realized if the non-self-complimentary linkers are shorter than the self-complementary linkers. In our simulation, the formed structures were less diverse than those in the experiment,<sup>5)</sup> which may be because we used a very simplified model: we neglected the differences in the particle size and interaction strength between the different species. If we take account of the differences, more diverse types of structures may be formed. We next intend to study the effect of these differences on the structures.

### Acknowledgments

This work was supported by JSPS KAKENHI Grant Numbers 26390054 and 16K05470. We were also supported by the Joint Research Program of the Institute of Low Temperature Science, Hokkaido University.

## References

- 1) D. Nykypanchuk, M. M. Maye, D. van der Lelie, and O. Gang, *Nature* **451**, 549 (2008).
- 2) S. Y. Park, A. K. R. Lytton-Jean, B. Lee, S. Weigand, G. C. Schatz, and C. A. Mirkin, *Nature* **451**, 553 (2008).
- 3) R. J. Macfarlane, B. Lee, H. D. Hill, A. J. Senesi, S. Seifert, and C. A. Mirkin, *Proc. Natl. Acad. Sci. U.S.A* **106**, 10493 (2009).
- 4) R. J. Macfarlane, B. Lee, M. R. Jones, N. Harris, G. C. Schatz, and C. A. Mirkin, *Science* **334**, 204 (2011).
- 5) C. Zhang, R. J. Macfarlane, K. L. Young, C. H. J. Choi, L. Hao, E. Auyeung, G. Liu, X. Zhou, and C. A. Mirkin, *Nat. Mater.* **12**, 741 (2013).
- 6) T. Isogai, A. Piednoir, E. Akada, Y. Akahosi, R. Tero, S. Harada, T. Ujihara, and M. Tagawa, *J. Cryst. Growth* **401**, 494 (2014).
- 7) T. Isogai, E. Akada, S. Nakada, N. Yoshida, R. Tero, S. Harada, T. Ujihara, and M. Tagawa, *Jpn. J. Appl. Phys.* **55**, 03DF11 (2016).
- 8) J. C. Crocker, *Nature* **451**, 528 (2008).
- 9) W. B. Rogers and J. C. Crocker, *Proc. Natl. Acad. Sci. U.S.A.* **108**, 15687 (2011).
- 10) H. Katsuno, Y. Maegawa, and M. Sato, *J. Phys. Soc. Jpn.* **85**, 074605 (2016).
- 11) D. L. Ermak, *J. Chem. Phys.* **62**, 4189 (1975).
- 12) P. J. Steinhardt, D. R. Nelson, and M. Ronchetti, *Phys. Rev. B* **28**, 784 (1983).
- 13) M. D. Rintoul and S. Torquato, *J. Chem. Phys.* **105**, 9258 (1996).
- 14) W. Mickel, S. C. Kapfer, G. E. Schröder-Turk, and K. Mecke, *J. Chem. Phys.* **138**, 044501 (2013).
- 15) P. G. Bolhuis, D. Frenkel, S. Mau, and D. A. Huse, *Nature* **388**, 235 (1997).